Acta Polytechnica **66**(1):30–35, 2026
https://doi.org/10.14311/AP.2026.66.0030

Published by the Czech Technical University in Prague

DESIGN AND STABILITY ANALYSIS OF A HIGH-PERFORMANCE THREE-PHASE INVERTER FOR PHOTOVOLTAIC APPLICATIONS

Mohammed El Bachir Ghribi[a, b, *], Zine Eddine Touhami Ternifi[b], Ghalem Bachir[b]

[a] *University of Sciences and Technology of Oran, Faculty of electrical engineering, Department of electrical engineering, Applied Power Electronics Laboratory (LEPA), Bir El Djir 1505, El-Mnaouer, 31000 Oran, Algeria*

[b] *University of Sciences and Technology of Oran, Faculty of electrical engineering, Department of electrical engineering, Laboratory of sustainable development of the electrical energy (LDDEE), Bir El Djir 1505, El-Mnaouer, 31000 Oran, Algeria*

[*] corresponding author: mohammedelbachir.ghribi@univ-usto.dz

Abstract. This paper presents the design and analysis of a three-phase photovoltaic inverter based on a Boost-Buck-Discharge microinverter architecture. It converts low DC voltages (24–240 V), typical of PV panels, into high-quality three-phase AC with minimal THD. The topology integrates a boost converter elevating voltage to 240 V, a buck-discharge stage generating rectified sinusoidal waveforms, and a full-bridge inverter producing pure sinusoidal outputs. A step-up transformer ensures standardised voltages of 225 V RMS (single-phase) and 390 V RMS (line-to-line) with galvanic isolation. Sliding mode control is applied to buck-discharge circuits to ensure robust and stable operation, validated via Lyapunov analysis. Results show THD below 3 % for all tested resistive and inductive loads, confirming efficient multilevel conversion and suitability for decentralised renewable energy systems requiring reliable three-phase DC-AC transformation.

Keywords: Photovoltaic, inverter, buck-discharge, sliding mode control, Lyapunov stability.

1. Introduction

The growth of renewable energy, particularly solar and wind, has greatly increased decentralised electricity generation, mainly through domestic photovoltaic systems whose output rarely exceeds a few kilowatts. This expansion requires adapting grids and converters to efficiently capture and inject this power with high quality, and developing conversion structures that transform DC energy into AC while maximising the injected power [1–6]. Photovoltaic installations, whether small or industrial, face a choice between centralised or string inverters – which simplify installation but reduce modularity and microinverters dedicated to individual panels. The latter limit power losses due to shading or failure, since the panels operate independently [7–9]. Modern inverter architectures in microinverters often employ multi-stage topologies designed to generate a sinusoidal voltage without the need for additional filtering. Primarily intended for low-power single-phase systems, these architectures include a front-end DC/DC stage to boost or modulate the input voltage. The resulting voltage is then converted into alternating current to supply a load or inject power into the grid, ensuring synchronisation and low harmonic distortion through optimised control [10–15]. Since a single solar panel rarely exceeds 50 V, modular inverters must boost this to 220–240 V AC. Achieving this requires a step-up transformer, which also ensures galvanic isolation between the source and the load [16, 17].

This work proposes a photovoltaic inverter based on a microinverter concepts, designed to deliver high-quality three-phase AC voltage and current with minimal harmonic distortion. It targets wide input voltages (24–240 V), ensuring compatibility with various batteries and PV systems. A multi-stage approach is adopted: the first stage is a boost converter to raise the voltage [18–22]; the second, a ripple system based on a buck-discharge structure [23]. Each phase uses a substructure producing a rectified sinusoidal voltage. The buck charges a capacitor, while the discharge circuit controls its release, yielding an asymmetric waveform approximating a sine. This waveform feeds a full-bridge inverter operating at grid frequency (50 Hz) in order to generate a pure sinusoidal output. At low input voltages, the transformer further increases voltage and provides galvanic isolation. The configuration is replicated for three phases, phase-shifted by $-120°$ and $-240°$, to ensure a balanced three-phase output. The buck-discharge circuit uses sliding mode control for its simplicity and compatibility with the converter's nonlinear behaviour, avoiding oscillations. The boost converter operates in open loop with a fixed duty cycle. Although the buck-discharge does not ensure perfect zero-crossing, slightly increasing THD, the impact one the total voltage remains minimal. Stability analysis confirms convergence, and results show THD below 3 % for all operating conditions, with transistor switching frequencies under 10 kHz.

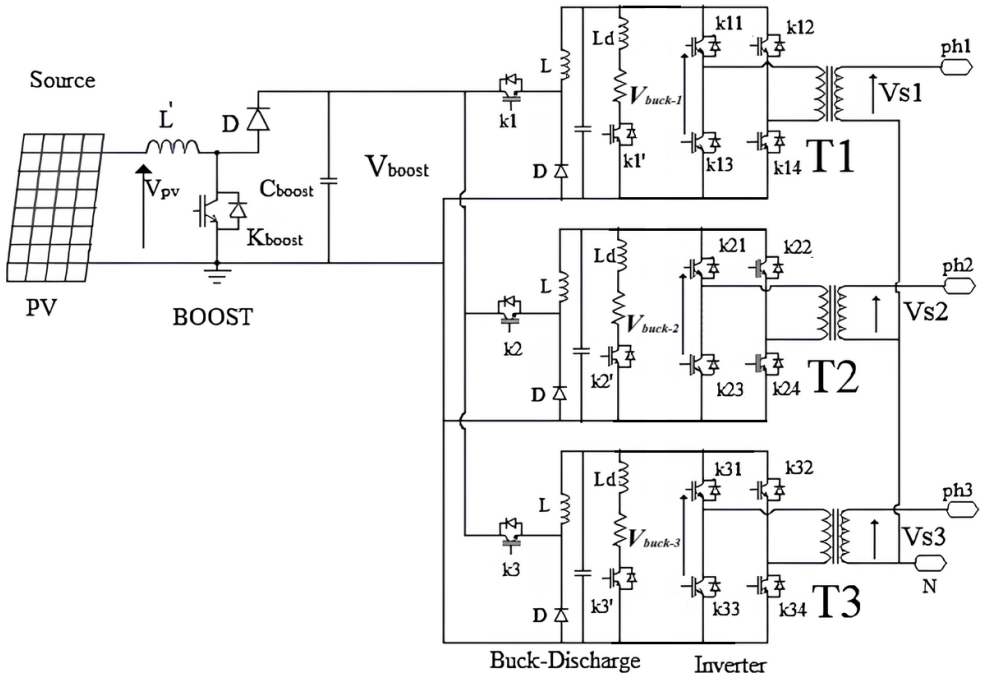

FIGURE 1. Schematic diagram of the high-performance boost-buck-discharge three-phase inverter.

2. MATERIALS AND METHODS

The schematic illustrated in Figure 1 presents the advanced architecture of a high-performance three-phase inverter derived from the boost-buck-discharge topology. This design aims to establish a benchmark in power conversion efficiency and reliability. The system starts with a boost converter that raises the input DC voltage (24–240 V) to a stable 240 V, ensuring compatibility with a wide range of sources. Subsequently, a buck converter operates in conjunction with a discharge circuit to generate a rectified sinusoidal waveform: the buck stage controls the capacitor charging process, while the discharge circuit governs the discharging phase to maintain voltage balance. The resulting waveform is then processed by a full-bridge inverter, converting it into a pure sinusoidal signal suitable for three-phase applications. A step-up transformer increases the voltage to 225 V RMS, ensuring compliance with standard output levels. Finally, the buck-boost and inverter stages are replicated to produce three phase-shifted voltages at 0°, −120°, and −240°, ensuring an efficient three-phase operation with minimal harmonic distortion.

The boost converter plays a crucial role in elevating the input voltage to a level suitable for the buck converter. Specifically, it increases the input voltage to the reference value of 240 V. This stage is managed through Pulse Width Modulation (PWM) control, which ensures precise regulation of the output voltage. A direct voltage measurement is employed to maintain accuracy. To optimise performance, the inductance and capacitance of the boost converter are carefully calculated. The capacitor is sized to supply the rated current to the inverter for one-quarter of the period, ensuring a sufficient energy storage and delivery. Concurrently, the inductor is designed to operate continuously with an acceptable ripple current rate, minimising losses and maintaining efficiency. The switching frequency of the boost converter is set to 5 kHz, a choice that balances efficiency with component stress and overall system performance. This frequency ensures that the converter operates effectively while keeping the ripple current within the acceptable limits, thus contributing to the overall high-quality output of the inverter system.

$$L' = \frac{V_{pv}\left(1 - \frac{V_{pv}}{V_{\text{boost}}}\right)}{4\,\Delta I_L f_s}, \tag{1}$$

$$C_{\text{boost-max}} = \frac{I_{\text{boost}}}{4\,\Delta V f_s}. \tag{2}$$

In the buck-discharge circuit, when switch K1 of the buck converter is activated, the capacitor begins to charge, causing the voltage across it to rise. Once the buck converter is deactivated, the capacitor discharges through both the load and the discharge circuits. The discharge inductor is utilised to limit the current flowing through the circuit when switch K1' is conducting. This combination of components produces a rectified sinusoidal waveform. The value of the discharge inductor (L_d) is designed to ensure that the maximum discharge current is not exceeded, particularly at minimal frequencies. To maintain optimal performance, the inductance (L_s) must satisfy the following inequality:

$$\frac{V_e - V_{\text{buck-max}}}{I_{\text{buck-max}} \times f_{\text{com-min}}} < L_s < \frac{V_{\text{buck-max}}}{I_{\text{buck-max}} \times f_{\text{com-min}}}. \tag{3}$$

The capacitor's role is to supply current to the load during the phase when the source is disconnected. To

maintain the same power output, a lower reference voltage for the buck converter necessitates a larger capacitor. This is because a lower voltage leads to higher inrush currents, increasing losses for undersised loads. The capacitor value is determined to supply the rated current to the load for one-quarter of the period:

$$C_{max} = \frac{I_c\,\Delta t}{\Delta V} = \frac{I_c}{4\,f_s\,\Delta V}. \tag{4}$$

The discharge inductance is calculated to ensure that the maximum discharge current is not exceeded, especially at minimal switching frequencies:

$$L_d < \frac{V_{\text{buck-max}}}{I_{L_d\text{-max}} \times f_{\text{com-min}}}. \tag{5}$$

The inverter is controlled using a sliding mode control (SMC) strategy, Each buck converter operates with its own reference voltage, phase-shifted by 120° from the others. To preserve efficiency and performance, the average switching frequency of the buck converters and discharge circuits is maintained below 10 kHz. The control law, expressed by Equation (6), corresponds to a first-order sliding mode control based on the sign function. Although this approach typically induces chattering in the controlled variable, in this system, the effect is negligible, as the converter naturally alternates between two switching states [24–26].

$$\begin{aligned}\alpha_j = {} & k_e \cdot \text{sign}(V_{\text{ref-}j} - V_{\text{buck-}j}) \\ & + k_n \int (V_{\text{ref-}j} - V_{\text{buck-}j})\,dt.\end{aligned} \tag{6}$$

For the stability analysis of the converter with the control law presented in Equation (6), the Lyapunov method is selected, as it is particularly well suited to nonlinear systems. Since the objective of the control is to regulate the three-phase system at the output, the most common Lyapunov function is a quadratic function of the voltage errors, given by Equation (7). The choice of this function is justified by its direct physical interpretation as an "error energy" that the system must dissipate. This approach ensures not only the stability of the equilibrium point but also the dynamic performance of the control loop [27–29].

$$V = \sum_{j=1}^{3} \frac{(V_{\text{ref-}j} - V_{\text{buck-}j})^2}{2}. \tag{7}$$

Condition one: The Lyapunov function is strictly zero at the origin:

$$V(0,0,0) = 0. \tag{8}$$

Condition two: The Lyapunov function is strictly positive:

$$V => 0. \tag{9}$$

Condition three: The derivative of the Lyapunov function is strictly negative. In demonstrating the sign of the derivative of the Lyapunov function, we assume that the reference is constant over a very short period of time:

$$\dot{V} = \sum_{j=1}^{3} -\dot{V}_{\text{buck-}j}(V_{\text{ref-}j} - V_{\text{buck-}j}). \tag{10}$$

For the control to remain stable, Condition 3 must be satisfied. To achieve this, the discharge branch, composed of switches k_1', k_2', and k_3', and the inverter bridge are considered as a simple load, which allows the direct consideration of the relationship between the input and the output of the buck converter to represent the operation of the buck-discharge stage. This simplification leads to the transition towards Equation (11) and implies that the variation of the duty cycle must have the same sign as the error, as shown in Equation (12):

$$\dot{V} = \sum_{j=1}^{3} -\dot{\alpha}_j V_{\text{boost}}(V_{\text{ref-}j} - V_{\text{buck-}j}) < 0, \tag{11}$$

$$\text{sign}(\dot{\alpha_j}) = \text{sign}(V_{\text{ref-}j} - V_{\text{buck-}j}). \tag{12}$$

By deriving the relation from Equation (6), it is possible to deduce the relationship between the error and the variation of the duty cycle, as given by Equation (13). This leads to Equation (14) and confirms that the sign of the variation of the duty cycle is identical to that of the error, thus validating Equation (12), ensuring control stability, and guaranteeing the convergence of the output voltage towards its reference value:

$$\begin{aligned}\dot{\alpha}_j = {} & -2k_e\dot{\alpha}_j V_{\text{boost}}\delta(V_{\text{ref-}j} - V_{\text{buck-}j}) \\ & + k_n(V_{\text{ref-}j} - V_{\text{buck-}j}),\end{aligned} \tag{13}$$

$$\dot{\alpha}_j = \frac{k_n(V_{\text{ref-}j} - V_{\text{buck-}j})}{1 + 2k_e V_{\text{boost}}\delta(V_{\text{ref-}j} - V_{\text{buck-}j})}. \tag{14}$$

This is then fed into a full-bridge inverter that translates the rectified sinusoidal voltage to an alternating sinusoidal waveform. To produce a high-quality output, the inverter operates with a 180° phase shift at a frequency of 50 Hz. All the inverters in the bridge are controlled 120° out of phase among each other, which results in a balanced three-phase output.

In this system, the purpose of the transformer is to step up the voltage from the inverter so it meets standardised output values. The transformer increases the single-phase voltage output to 225 V RMS, while increasing the voltage between two phases to 390 V RMS. This transformation of voltage provides an output that meets industry standards and is compatible with any application requiring steady and reliable power. The voltage is boosted to better manage power losses through the system and hence increase has a overall efficiency in such a way that the inverter has a high-quality sinusoidal output that meets the voltage specification for practical use.

The presented converter uses a total of nineteen power switches: twelve switches for the inverter

Parameter	Resistive load ($\phi = 0°$)		Inductive load ($\phi = 90°$)	
	RMS	THD	RMS	THD
Vs1	225.58 V	2.06 %	226.25 V	0.9 %
Vs2	225.56 V	1.98 %	226.24 V	0.32 %
Vs3	225.25 V	2.38 %	226.42 V	0.5 %
I1	2.25 A	2.06 %	2.25 A	1.60 %
I2	2.25 A	1.98 %	2.25 A	1.63 %
I3	2.25 A	2.38 %	2.25 A	1.83 %
V12	390.70 V	1.62 %	392.86 V	1.31 %
V23	390.70 V	1.75 %	391.99 V	1.40 %
V31	390.90 V	1.81 %	392.30 V	1.37 %

TABLE 1. Summary of results for the three-phase buck inverter in resistive and inductive load cases.

bridges, controlled by a square-wave signal at 180° with a frequency of 50 Hz, one switch for the boost converter, operated in an open loop at a frequency of 5 kHz with only the input voltage measured; and finally, each buck-discharge uses two power switches controlled asymmetrically, resulting in a total of six switches for the three buck-discharge circuits.

3. RESULTS AND DISCUSSION

These three buck-discharge circuits generate three rectified sinusoidal voltages, each phase-shifted by 120° with respect to the others, corresponding to the three phases of the system. In terms of THD, the performance, when the inverter is tested under resistive load, shows good voltage and line current THD, always staying below 3 %. This THD value is mainly due to the non-zero voltage during switching transitions in the bridge inverter for the line-to-line voltages. Zero-crossing is ensured for the line-to-line voltages, as these voltages are obtained from two single-phase voltages. Consequently, the THD of a line-to-line voltage remains below approximately 0.5 %. When tested with a purely inductive load, equivalent results were obtained, indicating robustness to load variations. Table 1 provides a summary of the THD values as well as the RMS values for various resistive and inductive loads, and it can easily be from this table that the nature of the load has a negligible impact on THD performance.

Figure 2 illustrates the output voltage of the buck-discharge circuit. It presents the waveform characteristics as well as the performance of the voltage generated by the buck converter coupled with the discharge circuit, highlighting the waveform that is close to the rectified sinusoid produced by the circuit. This figure provides an overview of the output voltage stability and quality. However, this type of converter struggles to ensure a perfect zero-crossing, particularly when the difference between the input and output voltages is significant, as is the case here. Figure 2 clearly shows this phenomenon, which decreases the THD but remains negligible for the line-to-line voltages. Figure 3 shows the voltage output from the

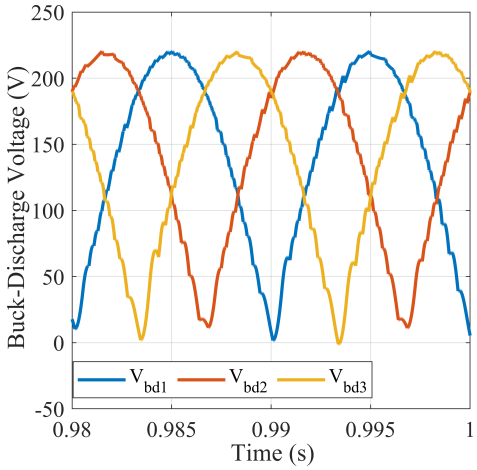

FIGURE 2. Buck-discharge Voltage Output.

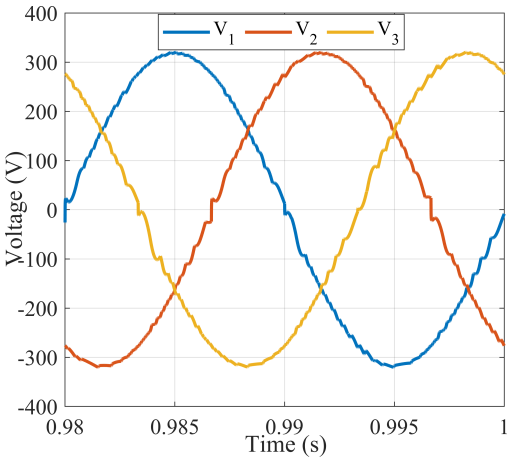

FIGURE 3. Voltage at the transformer output.

transformer, which follows the rectification and modulation stages of the inverter system. It shows the waveform of the voltage after being stepped up by the transformer to achieve the standardised values. The plot demonstrates the characteristics of the output voltage, including its amplitude and waveform shape, reflecting the effectiveness of the transformer in elevating the voltage to the required values of 225 V for single-phase and 390 V for inter-phase connections.

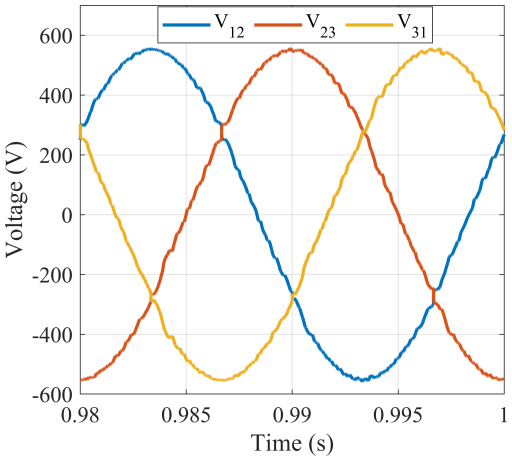

Figure 4. Complex three-phase voltage.

Figure 4 illustrates the complex three-phase voltage output of the inverter system. It presents the waveform of the three-phase voltage, showing the phase relationships and the overall shape of the voltage signal. The plot highlights how the individual phase voltages combine to form a balanced three-phase system, with each phase shifted by 120° from the others. The figure provides a comprehensive overview of the voltage quality and the synchronisation of the three phases in the system.

4. Conclusion

The proposed topology for the high-performance three-phase system exhibits excellent performance in terms of power quality. Thanks to the addition of the boost-buck-discharge mechanism, it achieves a THD below 3 % across a wide operating range. The use of a boost converter at the input allows for the utilisation of a wide variety of sources, ranging from a 24 V battery to a photovoltaic string of 240 V, The work presented in this document aims to propose a sizing method for the inverter, accompanied by a comprehensive study of the stability of the control applied to this topology using the Lyapunov method. The results obtained demonstrate good reference tracking and low THD, for loads ranging from pure resistance to pure inductance under nominal current.

List of symbols

$C_{\text{boost-max}}$ Boost capacitance [F]
$C_{\max}$ Buck-discharge capacitance [F]
f_s Synchronisation frequency [Hz]
$f_{\text{com-min}}$ Minimal switching frequency of buck converter [Hz]
I_1, I_2, I_3 Simple current [A]
L' Inductance of boost [H]
L_d Inductance of buck-discharge [H]
L_s Inductance of buck-discharge [H]
V_1, V_2, V_3 Simple voltage [V]
$V_{\text{ref-}j}, V_{\text{buck-}j}$ Buck converter reference voltage, buck converter voltage [V]
V_{12}, V_{23}, V_{31} Composite voltage [V]
V Lyapunov function

References

[1] A. J. Veldhuis, M. Leach, A. Yang. The impact of increased decentralised generation on the reliability of an existing electricity network. *Applied Energy* **215**:479–502, 2018. https://doi.org/10.1016/j.apenergy.2018.02.009

[2] M. Toloo, M. Taghizadeh-Yazdi, A. Mohammadi-Balani. Multi-objective centralization-decentralization trade-off analysis for multi-source renewable electricity generation expansion planning: A case study of Iran. *Computers & Industrial Engineering* **164**:107870, 2022. https://doi.org/10.1016/j.cie.2021.107870

[3] J. M. Weinand, F. Scheller, R. McKenna. Reviewing energy system modelling of decentralized energy autonomy. *Energy* **203**:117817, 2020. https://doi.org/10.1016/j.energy.2020.117817

[4] M. Ranjan, R. Shankar. A literature survey on load frequency control considering renewable energy integration in power system: Recent trends and future prospects. *Journal of Energy Storage* **45**:103717, 2022. https://doi.org/10.1016/j.est.2021.103717

[5] D. M. Scholten, N. Ertugrul, W. L. Soong. Micro-inverters in small scale PV systems: A review and future directions. In *2013 Australasian Universities Power Engineering Conference (AUPEC)*, pp. 1–6. IEEE, Australia, 2013. https://doi.org/10.1109/AUPEC.2013.6725465

[6] H. A. Sher, K. E. Addoweesh. Micro-inverters – promising solutions in solar photovoltaics. *Energy for Sustainable Development* **16**(4):389–400, 2012. https://doi.org/10.1016/j.esd.2012.10.002

[7] Q. Lagarde, B. Beillard, S. Mazen, et al. Performance ratio of photovoltaic installations in France: Comparison between inverters and micro-inverters. *Journal of King Saud University-Engineering Sciences* **35**(8):531–538, 2023. https://doi.org/10.1016/j.jksues.2021.11.007

[8] D. Kolantla, S. Mikkili, S. R. Pendem, A. A. Desai. Critical review on various inverter topologies for PV system architectures. *IET Renewable Power Generation* **14**(17):3418–3438, 2020. https://doi.org/10.1049/iet-rpg.2020.0317

[9] S. Deshpande, N. R. Bhasme. A review of topologies of inverter for grid connected PV systems. In *2017 Innovations in Power and Advanced Computing Technologies (i-PACT)*, pp. 1–6. IEEE, India, 2017. https://doi.org/10.1109/IPACT.2017.8245191

[10] M. A. Ismeil, H. S. Hussein, M. Nasrallah. Micro inverter grid connected for PV application based on SEPIC differential inverter. *SVU-International Journal of Engineering Sciences and Applications* **5**(1):1–12, 2024. https://doi.org/10.21608/svusrc.2023.224660.1142

[11] K. Janardhan, A. Mittal, A. Ojha. Performance investigation of stand-alone solar photovoltaic system with single phase micro multilevel inverter. *Energy Reports* **6**:2044–2055, 2020. https://doi.org/10.1016/j.egyr.2020.07.006

[12] J. Bauer. Single phase voltage source inverter photovoltaic application. *Acta Polytechnica* **50**(4):7–11, 2010. https://doi.org/10.14311/1217

[13] S. Danyali, O. Aghaei, M. Shirkhani, et al. A new model predictive control method for buck-boost inverter-based photovoltaic systems. *Sustainability* **14**(18):11731, 2022. https://doi.org/10.3390/su141811731

[14] V. H. Garcia-Rodriguez, J. H. Perez-Cruz, R. C. Ambrosio-Lazaro, S. Tavera-Mosqueda. Analysis of DC/DC boost converter – full-bridge buck inverter system for AC generation. *Energies* **16**(6):2509, 2023. https://doi.org/10.3390/en16062509

[15] L. Wang, C. Liu, J. Fang. Design of a single-stage transformerless buck–boost inverter for electric vehicle chargers. *Applied Sciences* **12**(13):6705, 2022. https://doi.org/10.3390/app12136705

[16] E. Płaczek-Popko. Top PV market solar cells 2016. *Opto-Electronics Review* **25**(2):55–64, 2017. https://doi.org/10.1016/j.opelre.2017.03.002

[17] G. R. Walker, P. C. Sernia. Cascaded DC-DC converter connection of photovoltaic modules. *IEEE Transactions on Power Electronics* **19**(4):1130–1139, 2004. https://doi.org/10.1109/TPEL.2004.830090

[18] P. Mašek. A new buck-boost converter for a hybrid-electric drive stand. *Acta Polytechnica* **49**(2):70–74, 2009. https://doi.org/10.14311/1129

[19] J. P. M. Figueiredo, F. L. Tofoli, B. L. A. Silva. A review of single-phase PFC topologies based on the boost converter. In *2010 9th IEEE/IAS International Conference on Industry Applications (INDUSCON)*, pp. 1–6. IEEE, Brazil, 2010. https://doi.org/10.1109/INDUSCON.2010.5740015

[20] B. M. Hasaneen, A. A. E. Mohammed. Design and simulation of DC/DC boost converter. In *2008 12th International Middle-East Power System Conference*, pp. 335–340. IEEE, Egypt, 2008. https://doi.org/10.1109/MEPCON.2008.4562340

[21] J. C. Rosas-Caro, J. M. Ramirez, F. Z. Peng, A. Valderrabano. A DC-DC multilevel boost converter. *IET Power Electronics* **3**(1):129–137, 2010. https://doi.org/10.1049/iet-pel.2008.0253

[22] Y. Hasuka, H. Sekine, K. Katano, Y. Nonobe. Development of boost converter for MIRAI. Tech. Rep. 2015-01-1170, SAE International, 2015. SAE Technical Paper. https://doi.org/10.4271/2015-01-1170

[23] M. E. B. Ghribi, Z. E. T. Ternifi, G. Bachir, M. Aillerie. Buck-based photovoltaic microinverter coupled to a discharge circuit. *Majlesi Journal of Electrical Engineering* **18**(1):323–333, 2024. https://doi.org/10.30486/mjee.2024.1992377.1189

[24] A. Leon-Masich, H. Valderrama-Blavi, J. M. Bosque-Moncusí, et al. Sliding-mode-control-based boost converter for high-voltage–low-power applications. *IEEE Transactions on Industrial Electronics* **62**(1):229–237, 2015. https://doi.org/10.1109/TIE.2014.2327004

[25] S.-C. Tan, Y. M. Lai, C. K. Tse. Indirect sliding mode control of power converters via double integral sliding surface. *IEEE Transactions on Power Electronics* **23**(2):600–611, 2008. https://doi.org/10.1109/TPEL.2007.915624

[26] J. Bauer. Simulation of a matrix converter fed drive with sliding mode control. *Acta Polytechnica* **52**(5):8–16, 2012. https://doi.org/10.14311/1620

[27] A. M. Lyapunov. The general problem of the stability of motion. *International Journal of Control* **55**(3):531–534, 1992. https://doi.org/10.1080/00207179208934253

[28] C. S. T. Dong, H. H. Vo, T. C. Tran, et al. Application of sensorless sliding mode observer in control of induction motor drive. *Advances in Electrical and Electronic Engineering* **15**(5):747–753, 2017. https://doi.org/10.15598/aeee.v15i5.2626

[29] M. Ateş, S. Laribi. New results on the global asymptotic stability of certain nonlinear RLC circuits. *Turkish Journal of Electrical Engineering and Computer Sciences* **26**(1):434–441, 2018. https://doi.org/10.3906/elk-1612-100